Sep 25th, 2:10 PM

Improvement of Lithium-Metal Electrode All-Solid-State Batteries Performance by Shot Peening and Magnetron Sputtering

Atsuro Okumura
Institute of Science Tokyo

Manabu Kodama
Institute of Science Tokyo

IMPROVEMENT OF LITHIUM-METAL ELECTRODE ALL-SOLID-STATE BATTERIES PERFORMANCE BY SHOT PEENING AND MAGNETRON SPUTTERING

Atsuro Okumura[1], Hito Fukusumi[1] and Manabu Kodama[1]

1 Department of Mechanical Engineering, School of Engineering, Institute of Science Tokyo, Ookayama 2-12-1, Meguro-ku, Tokyo 152-8550, Japan

Abstract

To enable fast charging in lithium-metal anode all-solid-state batteries, suppressing lithium dendrite formation at the solid electrolyte (SE) interface is critical. Increasing fracture toughness via shot peening (SP) and improving interfacial contact with Au sputtering can inhibit dendrite growth. However, conventional sputtering may reduce toughness due to localized thermal damage. This study investigated magnetron sputtering as a low-damage, plasma-based Au deposition method. SEs with and without SP were fabricated and coated via normal and magnetron sputtering. Critical current density (CCD) and fracture toughness were evaluated. Without SP, CCD improvement was limited regardless of sputtering method due to poor bonding. With SP, CCD was significantly enhanced, and magnetron sputtering yielded higher CCD than conventional sputtering. Fracture toughness tests confirmed that thermal damage from normal sputtering reduced strength, while magnetron sputtering preserved it. These findings demonstrate that combining SP with magnetron sputtering improves SE interfacial properties, enhancing fast-charging capability and cycling stability.

Keywords All-solid-state battery, Oxide solid electrolyte, Shot peening, Magnetron sputtering, Critical current density, Fracture toughness

Introduction

To promote carbon neutrality, the development of safer and higher-capacity batteries for electric vehicles is essential. Conventional lithium-ion batteries rely on organic liquid electrolytes, which pose a risk of ignition. As a promising alternative, all-solid-state lithium-ion batteries (ASSLiBs) employ flame-retardant inorganic solid electrolytes (SEs), offering improved safety. Furthermore, the use of lithium-metal anodes in ASSLiBs can significantly enhance energy density because the theoretical capacity of lithium metal is nearly 10 times greater than that of graphite [1,2]. However, under high-rate charging conditions, lithium dendrites tend to form within the SE, leading to internal short circuits and limiting the critical current density (CCD) [3]. Therefore, strategies to suppress dendrite growth and enhance interfacial properties are crucial for realizing fast-charging ASSLiBs.

Among these strategies, shot peening (SP) has been reported to be effective in improving the mechanical durability of the SE surface. It has been experimentally demonstrated that SP improves the fracture toughness of the SE surface. Fracture toughness is a key property that characterizes a material's resistance to crack propagation [4], which is important because lithium dendrites tend to grow along such cracks in brittle SEs. Enhancing fracture toughness via SP is thus considered an effective way to suppress dendrite growth.

To further improve the electrochemical contact between the lithium-metal anode and the SE, inserting a metal interlayer such as gold (Au) has also proven useful. Temporary alloying between the Au layer and lithium promotes uniform interfacial reactions and improves contact [5]. Sputtering is widely used to deposit such metal layers due to the high purity and uniformity of the resulting thin films. In this process, plasma generated by high-voltage discharge accelerates cations to bombard a metal target, ejecting atoms for deposition onto the substrate [6].

Previous studies have shown that the combination of SP and Au sputtering greatly enhances CCD, far beyond what either treatment can achieve alone. For instance, Au sputtering onto an SP-treated SE surface led to a charging rate nearly 20 times faster than that without SP

[7]. These results demonstrate that SP is not simply an auxiliary process, but serves as an essential factor in realizing fast-charging ASSLiBs.
However, in conventional sputtering, the generated plasma is also present near the SE surface. Fig.1(a) shows the generated plasma during normal sputtering. This plasma can potentially cause thermal damage that degrades the fracture toughness of the SE and diminishes the effect of SP [7]. To address this issue, this study employed magnetron sputtering. Fig.1(b) shows the generated plasma during magnetron sputtering. In this technique, a magnet installed inside the top electrode generates a magnetic field that confines dense plasma near the metal target (Fig. 1(b)) [8]. As a result, only dilute plasma reaches the SE surface, which may reduce thermal damage and help preserve the enhanced fracture toughness imparted by SP.
In this study, we investigated the effects of Au deposition by magnetron sputtering on the fracture toughness of SEs and examined the correlation with CCD to evaluate the improvement in the charging performance of oxide-based lithium-metal anode ASSLiBs. Specifically, SEs with and without SP treatment were prepared and coated with Au via both normal and magnetron sputtering. CCD tests and fracture toughness measurements were then performed to assess how the combination of SP and low-damage sputtering affects interfacial properties and fast-charging capability.

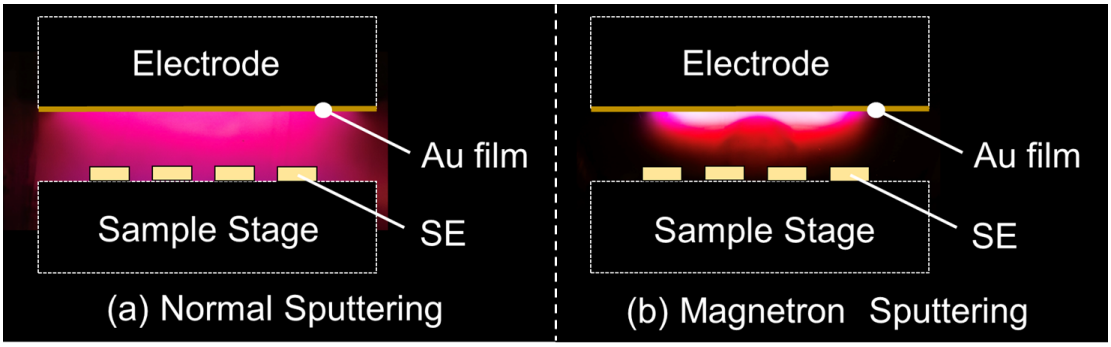

Figure 1. Plasma images obtained during (a) normal sputtering and (b) magnetron sputtering.

Experimental Procedures or Computational Methods

1 Material synthesis

The solid electrolyte employed was a Ga-substituted garnet-type oxide, $Li_{6.25}Ga_{0.25}La_3Zr_2O_{12}$ (LGLZO). Gallium doping has been reported to facilitate the formation of the desired cubic phase and achieve a dense microstructure with ease [9]. The synthesis procedure for LGLZO involved the following steps. Stoichiometric amounts of La_2O_3 (99.9%, Kojyundo Chemicals), ZrO_2 (98%, Kojyundo Chemicals), Ga_2O_3 (99.99%, Wako Chemicals), and LiOH (98%, Alfa Aesar) were weighed and mixed in a magnetic agate mortar at 100 rpm for 5 minutes. Subsequently, the blended powder (18 g) was separated into two 50 mL zirconia containers (Ito Seisakusho), to which 20 zirconia balls (10 mm and 5 mm in diameter) and 30 mL of hexane (95%, Hayashi Pure Chemical) were added. Ball milling was performed at 300 rpm for 2 hours. The resultant slurry was dried using a hot plate followed by vacuum drying, and the powder was transferred to a 25 mL platinum crucible (Tanaka Kikinzoku Kogyo) and calcined at 800 °C for 12 hours in an electric furnace (CWF13/5, CARBOLITE GERO), with a heating rate of 5 °C/min and cooling rate of 2 °C/min. The calcined solid was pulverized with a stainless-steel mortar and pestle, ball milled again, and dried under identical conditions. The resulting powder was compacted into 5 mm diameter pellets at 150 MPa using a hydraulic press (TB-20H, Sansho Industries). To sinter the pellets, they and the sieved mother powder were layered into a platinum crucible and heated at 1050 °C for 12 hours in the same furnace, maintaining the same heating and cooling rates. After sintering, the pellets were ground into the final shape using a leutor, and their surfaces were polished with 1500 grit sandpaper in air, resulting in LGLZO pellets measuring 4 mm in diameter and 1 mm in thickness.

2 Shot peening on solid electrolyte surface

Fig. 2 illustrates the shot peening (SP) process applied to an SE pellet. SP was applied to both surfaces of the solid electrolyte pellets in the air. The SP media consisted of angular Al_2O_3 particles with a mean diameter of 50 μm, propelled by compressed air from a compressor (MCP-25SLMA, Monotaro). The nozzle-to-sample distance was set at 10 cm, with the air pressure fixed at 0.4 MPa, and the treatment time was 10 seconds. After SP, compressed air without any media was used to clean off any residual particles from the SE surface.

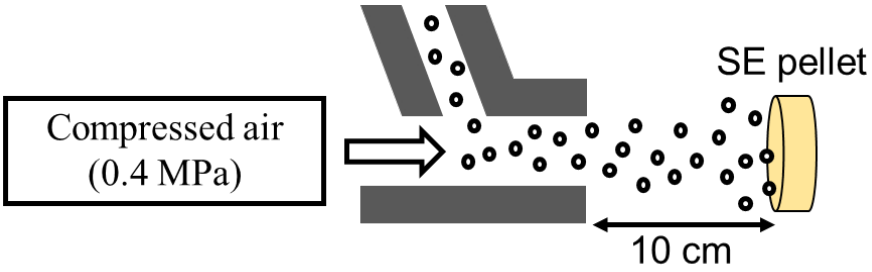

Figure 2. Schematic of shot peening of an SE pellet.

3 Au film formation on SE surfaces by sputtering

Thin Au films (approximately 200 nm) were deposited onto the surfaces of the SE pellets using two sputtering methods: normal sputtering (SC-701Mk II, Sanyu Electron) and magnetron sputtering (SC-701HMC, Sanyu Electron). Despite using different devices, the electrode dimensions and electrode spacing were comparable; the main distinction was the application of a magnetic field in the magnetron setup. The deposition rates were measured using ultra-small-angle X-ray scattering by comparing the transmission intensities through untreated Kapton tape and Kapton tape sputtered for 10 min. The measured rates were 14.03 nm/min for normal sputtering and 30.33 nm/min for magnetron sputtering. Based on these values, the sputtering durations were adjusted to achieve a film thickness of approximately 200 nm: 16 min for normal sputtering and 7 min 24 s for magnetron sputtering. To prevent Au deposition on the pellet sides, which could lead to electrical shorting, the top edges were masked using a metal plate with 5 mm diameter holes and copper tape with 3.2 mm diameter holes. Both sputtering processes were conducted under vacuum, with argon gas introduced after evacuation. The ion current was stabilized by adjusting the argon gas flow to maintain consistent chamber conditions during film deposition.

4 Measurement of the CCD

Symmetric lithium cells were fabricated using the surface-modified SEs, and the charging performance was evaluated [10]. Circular lithium foils (4-mm-diameter) were attached to each side of the SE in an argon-filled glove box with low moisture and oxygen levels, considering lithium's high reactivity. These symmetric cells were mechanically pressed with a spring-loaded fixture, applying a constant pressure of 5 MPa by adjusting the screw tightener to control the spring's deflection. The assembled cells were then enclosed in hermetically sealed containers filled with argon and desiccant to prevent moisture ingress during testing outside the glove box. In the critical current density (CCD) evaluation, the current density was incrementally increased until cell shorting occurred. Higher CCD values indicate more effective suppression of lithium dendrite growth. In stable lithium deposition, the voltage increases proportionally with current density, whereas a sudden voltage drop signifies dendrite-induced shorting. Measurements were performed using a charge–discharge tester (EF-7100P, Electrofield) inside a thermostatic chamber (SU-241, ESPEC Corp.) held at 60 °C. Testing commenced 2 hours after chamber insertion to ensure thermal equilibrium.

5 Measurement of the fracture toughness

Fracture toughness of the SE surface was measured by indentation using a Vickers hardness tester (HM-201C, Mitutoyo), followed by SEM observation (TM-4000, Hitachi High-Tech). The fracture toughness, Kc, was calculated using Eq. 1 below [11], based on the indenter load, crack lengths extending from the indentation corners, and Young's modulus:

$$K_c = 0.026 \frac{E^{\frac{1}{2}} P^{\frac{1}{2}} a}{c^{\frac{3}{2}}} \qquad (1)$$

where E is the Young's modulus (130 GPa for LLZO) [12], P is the applied load in newtons, a is the mean half-diagonal of the indentation, and c is the mean half-length of the radial cracks, all expressed in meters. An indenter load of 1 kgf was used.

Results

To assess how SP and magnetron sputtering influences the charging capability of lithium symmetric cells, both critical current density (CCD) tests and fracture toughness evaluations were conducted on solid electrolytes (SEs) subjected to six distinct surface modification procedures. Fig. 3 illustrates the individual processes corresponding to each sample. Sample A was prepared by surface smoothing using sandpaper only. For Sample B, shot peening (SP) was applied after surface smoothing. Sample C received a 200 nm Au film by normal sputtering after surface smoothing. Sample D received a 200 nm Au film by magnetron sputtering after surface smoothing. Sample E was processed with surface smoothing, SP, and subsequently normal sputtering. Sample E was processed with surface smoothing, SP, and subsequently magnetron sputtering. While all procedures took place in the air, the SEs were generally stored in an argon-filled glove box and exposed to the atmosphere only during processing. The exposure time was roughly 10 minutes for surface smoothing only, and about 30 minutes for sanding followed by SP. The sputtering itself occurred in an argon atmosphere and was thus excluded from the atmospheric exposure duration. After each procedure, SE samples were promptly returned to the glove box.

Fig. 4 shows the 3D SEM images of Samples A and B. As shown in (a), Sample A exhibits faint traces from the surface smoothing using sand paper. For Sample B in (b), SP treatment produced a textured surface with approximately 1.05 μm of roughness. Previous findings

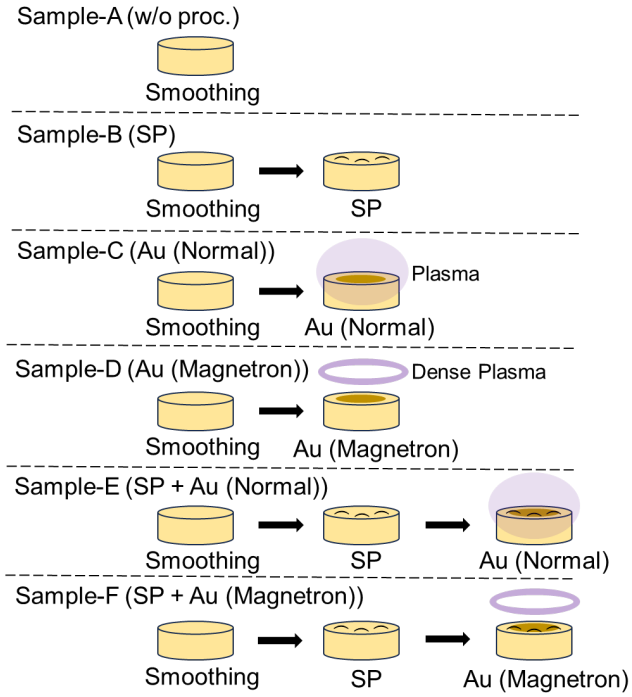

Figure 3. Illustration of the six processes employed for preparing the SE samples.

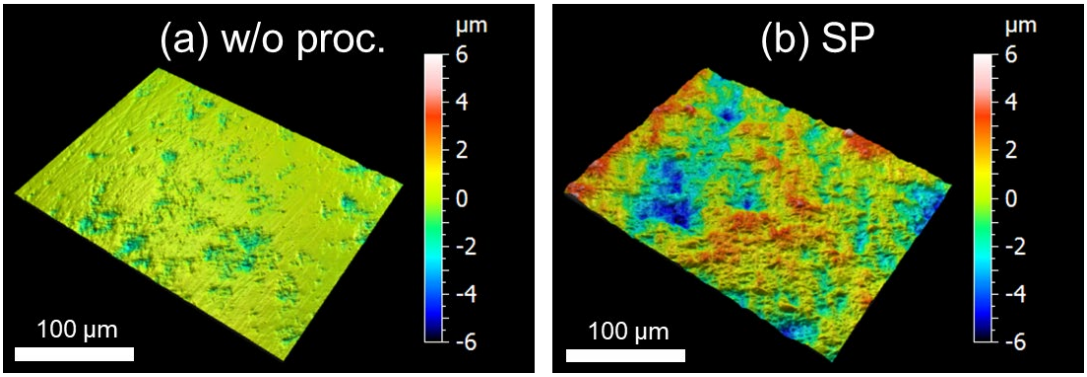

Figure 4. The SE surface 3D SEM images of (a) the sample without processing and (b) the sample treated with SP.

under similar SP conditions confirmed that the roughness-induced surface area increase was under 10% and unlikely to cause electrical field concentration [7]. Additionally, it is important to investigate whether the Al_2O_3 media used during SP remain on the SE surface. Prior studies utilizing Auger spectroscopy under identical SP conditions found no detectable alumina layer, indicating that Al_2O_3 particles used during SP do not interfere with electrochemical performance [7].

1 CCD results for each condition

Fig. 5 shows the polarization responses obtained from CCD experiments for each surface treatment. Under all conditions, a distinct voltage drop was observed at a certain current density, marking the onset of short-circuiting due to lithium dendrite penetration into the counter electrode. Since electronic conductivity within dendrites is significantly higher than ionic conductivity through the SE, this leads to a rapid voltage collapse once shorting occurs [13].

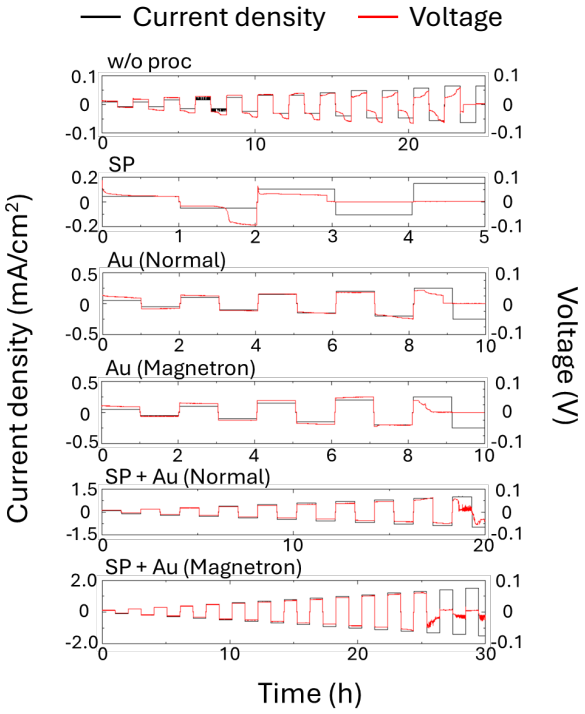

Figure 5. Polarization curves of the six tested samples.

The results without SP are summarized in Fig. 6(a) for three surface conditions: untreated, Au deposition by normal sputtering, and Au deposition by magnetron sputtering. Au coating enhanced CCD values in general, but no noticeable difference was observed between the two sputtering approaches, with both showing around 0.2 mA/cm². The results with SP are summarized in Fig. 6(b) for three surface conditions: without sputtering, Au deposition by normal sputtering, and Au deposition by magnetron sputtering. Here, CCD was clearly improved by Au coatings, and magnetron sputtering in particular showed a marked increase. The CCD reached ~0.93 mA/cm² for normal sputtering and ~1.35 mA/cm² for magnetron sputtering after SP treatment, suggesting a substantial enhancement in charge endurance.
SP alone enhanced CCD by nearly fourfold compared to untreated surfaces. This indicates that the mechanical reinforcement imparted by SP contributes meaningfully to lithium deposition behavior. While there was little difference between sputtering types without SP, after SP, magnetron sputtering resulted in significantly better CCD values. Accordingly, we examined how each surface treatment impacted the mechanical robustness of the SE surface by evaluating fracture toughness.

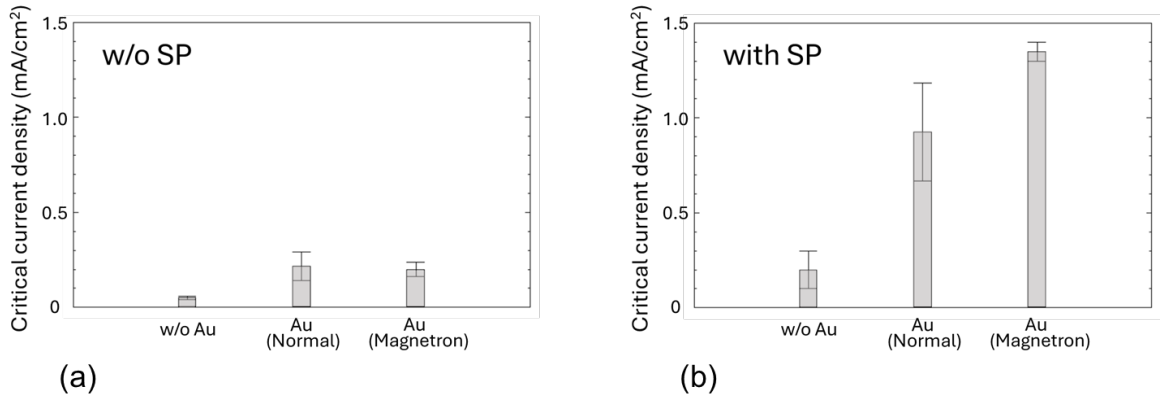

Figure 6. The CCD obtained (a) without SP and (b) with SP.

2 Fracture toughness results for each condition

To evaluate surface mechanical integrity, indentation-based fracture toughness tests were carried out. Fig. 7 illustrates representative crack and indentation patterns on SEs coated with Au thin films using Vickers indentation. Measurements (n = 6) were made under various surface treatment conditions, with crack lengths and indent dimensions obtained from 3D SEM analysis.
Fig. 8(a) indicates fracture toughness among the three surface treatments without SP: no Au coating, Au coating by normal sputtering, and by magnetron sputtering. The fracture toughness values were uniformly low across all three, indicating that sputtering alone did not alter mechanical properties. This finding corresponds with the CCD trends shown in Fig. 5(a), where sputtering type had minimal influence.
Fig. 8(a) indicates fracture toughness among the three surface treatments with SP: no Au coating, Au coating by normal sputtering, and by magnetron sputtering. Although SP alone improved surface toughness, applying normal sputtering afterward significantly reduced it. This reduction was likely caused by thermal effects resulting from plasma contact. In contrast, magnetron sputtering caused only a slight reduction, possibly because the magnetic field confines the dense plasma near the target and results in lower plasma density at the SE surface. The more moderate decline observed with magnetron sputtering may be due to the absence of substantial prior toughness enhancement, such as that achieved by SP, which limited the extent of thermal damage from the plasma.

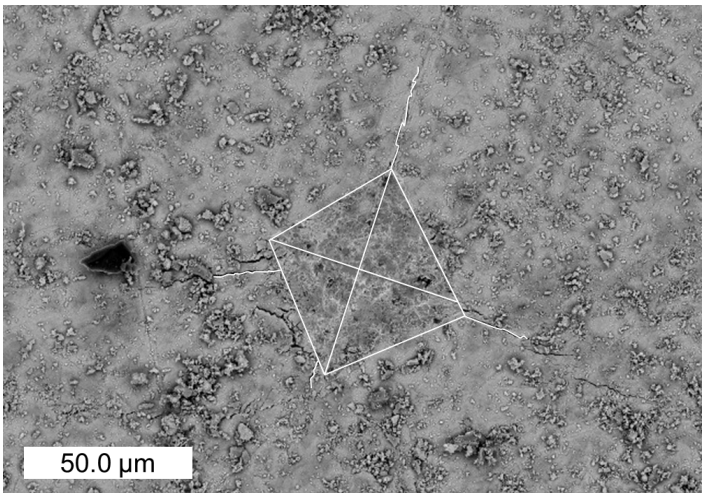

Figure 7. Images of the crack and the indentation on the SE surface.

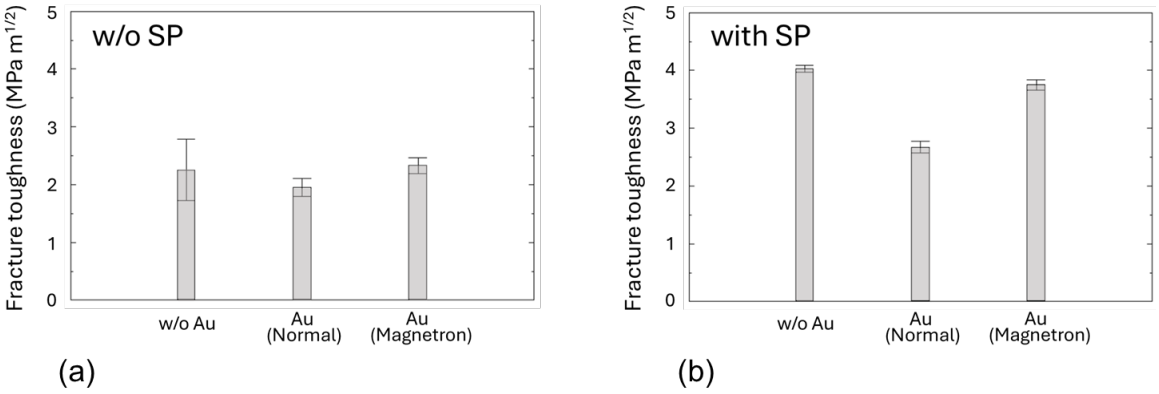

Figure 8. Fracture toughness of the SE surfaces (a) without SP and (b) with SP.

Despite the minor loss in fracture toughness, CCD was still substantially improved by magnetron sputtering compared to normal sputtering (Fig. 6(b)). This implies that introducing a low-damage Au interlayer via magnetron sputtering is effective for improving charging performance, without compromising the fracture toughness improvement resulting from SP.

Discussion and Conclusions

To improve the charging performance of all-solid-state lithium batteries (ASSLiBs) with lithium-metal anodes, we explored an alternative approach for Au film deposition. In particular, both normal and magnetron sputtering techniques were employed on solid electrolytes (SEs), with or without prior shot peening (SP), and their effects were evaluated via critical current density (CCD) testing and fracture toughness analysis. Magnetron sputtering, which confines sputtered atoms using magnetic fields, enables low-damage deposition by concentrating energetic species near the metal target rather than the substrate. This technique facilitates the formation of an Au coating that inhibits lithium dendrite growth while preserving the SE surface strength, thereby further reducing dendrite growth.

Without SP, Au coating moderately enhanced the CCD, but no substantial difference was found between the two sputtering methods. Similarly, fracture toughness remained comparable under all conditions, indicating that the original SE material's inherently low toughness was not adversely affected by either sputtering method. However, with SP, magnetron sputtering significantly increased the CCD and retained the improved fracture

toughness conferred by SP. Conversely, normal sputtering degraded the benefits of SP, likely due to thermal damage from the plasma.
These findings underscore that magnetron sputtering enables Au deposition with minimal mechanical compromise, effectively enhancing CCD performance. As a result, the synergistic use of SP and magnetron sputtering represents a promising strategy for boosting the charging performance of ASSLiBs employing lithium-metal anodes.

References

[1] J. Wang, Q. Zheng, M. Fang, S. Ko, Y. Yamada, A. Yamada, Advanced Science, 8 (2021), 2101646.

[2] X. Zhang, C. Sun, Chemistry Letters, 51 (2022), 891–894.

[3] B. Wu, S. Wang, J. Lochala, D. Desrochers, B. Liu, W. Zhang, J. Yang, J. Xiao, Energy & Environmental Science, 11 (2018), 1803–1810.

[4] G.D. Quinn, Mechanical Properties and Performance of Engineering Ceramic Engineering Ceramics II: Ceramic Engineering and Science Proceedings, 27 (2006), Chapter 5.

[5] J. Wakasugi, H. Munakata, K. Kanamura, J. Electrochem. Soc., 164 (2017), A1022–A1027.

[6] R. Grag, S. Gonuguntla, S. Sk, M.S. Iqbal, A.O. Dada, U. Pal, M. Ahmadipour, Advances in Colloid and Interface Science, 330 (2024), 103203.

[7] M. Kodama, K. Takashima, S. Hirai, Journal of Power Sources, 537 (2022), 231556.

[8] P.J. Kelly, R.D. Arnell, Vacuum, 56 (2000), 159–172.

[9] M. Mishra, C.W. Hsu, P.C. Rath, J. Patra, H.Z. Lai, T.L. Chang, C.Y. Wang, T.Y. Wu, T.C. Lee, J.K. Chang, Electrochimica Acta, 353 (2020), 136536.

[10] M. Klimpel, H. Zhang, M.V. Kovalenko, K.V. Kravchyk, Communications Chemistry, 6 (2023), 192.

[11] C.B. Ponton, R.D. Rawlings, Materials Science and Technology, 5 (1989), 865–872.

[12] J.E. Ni, E.D. Case, J.S. Sakamoto, E. Rangasamy, J.B. Wolfenstine, Journal of Materials Science, 47 (2012), 7978–7985.

[13] M. Siniscalchi, Y. Shi, G. Li, J.S. Gibson, R.S. Weatherup, R.S. Bonilla, S.C. Speller, C.R.M. Grovenor, Energy & Environmental Science, 7 (2024), in press.